INSTITUTE OF PHYSICS PUBLISHING PLASMA SOURCES SCIENCE AND TECHNOLOGY

Plasma Sources Sci. Technol. **14** (2005) 477–484 doi:10.1088/0963-0252/14/3/009

Chamberless plasma deposition of glass coatings on plastic

G R Nowling[1], M Yajima[1], S E Babayan[2], M Moravej[1], X Yang[1], W Hoffman[3] and R F Hicks[1]

[1] Chemical Engineering Department, University of California, Los Angeles, CA 90095, USA
[2] Surfx Technologies LLC, 3617 Hayden Avenue, Culver City, CA 90232, USA
[3] Motorola Advanced Technology Center, 1301 E. Algonquin Road, Schaumburg, IL 60196, USA

E-mail: rhicks@ucla.edu

Received 10 August 2004, in final form 20 December 2004
Published 23 May 2005
Online at stacks.iop.org/PSST/14/477

Abstract

A chamberless, remote plasma deposition process has been used to coat silicon and plastic substrates with glass at ambient conditions. The films were deposited by introducing an organosilane precursor into the afterglow of an atmospheric plasma fed with helium and 2 vol% oxygen. The precursors examined were hexamethyldisilazane, hexamethyldisiloxane, tetramethyldisiloxane, tetramethylcyclotetrasiloxane and tetraethoxysilane. With hexamethyldisilazane, glass films were deposited at rates of up to 0.25 μm min^{-1} and contained as little as 13.0 mol% hydroxyl groups. These films exhibited low porosity and superior hardness and abrasion resistance. With tetramethyldisiloxane, glass films were deposited at rates up to 0.91 μm min^{-1}. However, these coatings contained significant amounts of carbon and hydroxyl impurities ($\sim$20 mol% OH), yielding a higher density of voids and poor abrasion resistance. In summary, the properties of glass films produced by remote atmospheric plasma deposition strongly depend on the organosilane precursor selected.

1. Introduction

The use of plastic in place of glass or metal components is of great interest in consumer electronics. For example, the weight of flat panel displays would decrease substantially upon substituting plastic for glass screens [1]. Plastic housings are widely used in cell phones, PDAs, digital cameras and other handheld devices. In addition, new electronic products are being developed that are based almost completely upon polymeric materials. Two notable examples are flexible displays embedded with organic light emitting diodes and CMOS devices patterned onto plastic substrates [2–5]. One of the principal drawbacks of these materials is their poor resistance to scratching and abrasion, which reduces the useful life of the product. This problem can be overcome by depositing scratch-resistant films, such as glass (SiO_2), onto the plastic surface [6].

Plasma-enhanced chemical vapour deposition (PECVD) is a promising technique for coating thermally sensitive materials. This technique consists of mixing a volatile precursor with a plasma discharge and directing the reactive mixture onto the substrate surface [7]. High-quality glass has been deposited on plastic at rates ranging up to 6.0 μm min^{-1} [8–11]. Nevertheless, these processes were carried out in batch vacuum systems, which are not suitable for continuous in-line processing of large sheets or three-dimensional objects.

In this paper, we describe an atmospheric plasma process that operates without a chamber so that there is no limitation on the substrate size or dimensions. The plasma generates O, N, or H atoms at concentrations near 10^{16} cm^{-3} at temperatures between 70°C and 120°C [12–17]. This device has been used to deposit silicon nitride and amorphous hydrogenated silicon on glass and silicon wafers inside a reactor vessel [17, 18]. Herein, we examine the chamberless remote deposition of abrasion-resistant glass coatings on plastic. It has been found that the film growth rate, composition and hardness depend on the choice of the organosilane precursor and its partial pressure in the feed.

2. Experimental methods

The apparatus used in this study was an Atomflo™ 250D coating tool from Surfx Technologies LLC. A schematic of the set-up is shown in figure 1. Oxygen, 2.0 vol%, and helium were fed to the capacitive discharge plasma that was driven by 100 W of radio frequency power at 27.12 MHz. The precursor was introduced separately in helium carrier gas to a showerhead attached just downstream of the electrodes. The area of the showerhead was 5.1 cm^2, and the total flow rate was 30.6 litre min^{-1} at 25°C and 1 atm. The substrates were placed 2.75 mm downstream of the showerhead and spun at a rate of 6.0 rpm. In addition, the plasma deposition source oscillated horizontally ±2.25 mm over the rotating sample at a rate of 3.9 mm s^{-1}. The substrates were not heated other than by the plasma gas.

Five silicon precursors were examined over the course of this study: hexamethyldisilazane (HMDSN), hexamethyldisiloxane (HMDSO), tetramethyldisiloxane (TMDSO), tetramethylcyclotetrasiloxane (TMCTS) and tetraethoxysilane (TEOS). The properties of each precursor are listed in table 1. The vapour pressures of TMCTS, TEOS and HMDSN were taken from product literature [19–21], while the vapour pressures of TMDSO and HMDSO at the bubbler temperatures were estimated using the Clausius–Clapeyron equation and published vapour pressures at other temperatures [22–24].

The glass films were deposited on silicon substrates and then analysed for film thickness, composition and structure. The substrates were n-type Si (1 0 0) squares, 3.8 × 3.8 cm^2. An ellipsometer (SCI FilmTek 2000) was used to measure the film thickness and the refractive index at $\lambda = 632$ nm. The values reported herein are the averages of 15 data points across the film. The standard deviation of the thickness was ±8%. The deposition rate was determined by dividing the average film thickness by the process time. The film thickness obtained via this technique was verified using a step profiler (Veeco Instruments Dektak 8). The step was created by coating half of the film with a silicone adhesive sealant (GE Translucent RTV 108) and etching the unmasked region away by immersing the sample in a 10% HF solution. Finally, the adhesive was removed with acetone. Several films of varying thicknesses and compositions were tested in this fashion, and all exhibited thicknesses within the standard deviation of the values determined by ellipsometry. Film composition was examined by infrared (IR) spectroscopy using a Bio-Rad FTS-40A with a DTGS detector. The IR spectra of the films were taken after 48 to 72 h of exposure to the atmosphere [25]. Absorbance spectra were obtained by taking the ratio of scans recorded before and after film deposition. Finally, the film morphology was analysed with a three-dimensional optical surface profiler (Nano-Or 3DScope 2000 SEMI).

Preliminary scratch tests were performed on films deposited on silicon wafers. Samples were scratched with the corner of a 3/8 inch blade screwdriver held ∼45° from the surface normal. The blade corner was pressed firmly onto the film and dragged along the surface. The resulting scratch was rated as either shallow or deep. 'Shallow' scratches were barely visible to the eye and were less than 13 nm in depth, as measured by the step profiler. 'Deep' scratches were easily seen with the eye and penetrated at least 200 nm into the film. It should be noted that these tests provided only a qualitative comparison of the deposition results. Further quantitative mechanical tests were performed on films deposited on 2.5 × 2.5 cm^2 pieces of LEXAN® EXL1414 thermoplastic [26]. The hardness was determined using the pencil test [27, 28], while the abrasion resistance was characterized by rubbing the samples with steel wool and counting the number of scratches seen with an optical microscope.

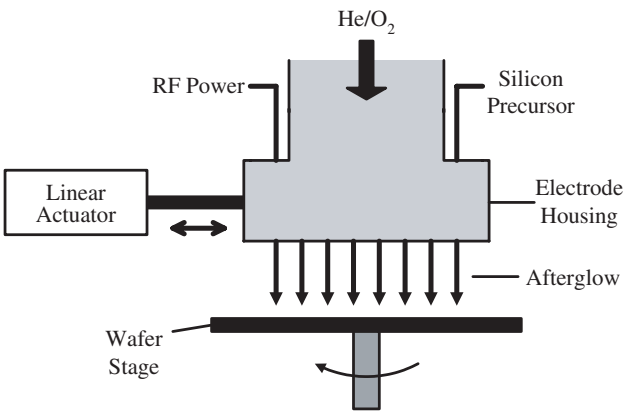

Figure 1. Schematic of the chamberless atmospheric plasma deposition apparatus.

3. Results

3.1. Deposition rate trends

In figure 2, the deposition rates observed for each of the five precursors are plotted as a function of their partial pressure in the feed. The inlet pressures were varied by changing the helium flow rate through the bubbler, while holding the bath temperature constant at the values listed in table 1. The maximum flow rates through the bubblers were 50 sccm for TMDSO, 120 sccm for HMDSN and HMDSO and 1000 sccm for TMCTS and TEOS. It is assumed that at these flow rates the vapour achieved saturation in the helium carrier gas.

Table 1. Properties of the organosilane precursors used in this study.

Name	Molecular weight	Chemical formula	Bubbler temp. (°C)	Vapour pressure (Torr)
Hexamethyldisilazane	161.4	$C_6H_{19}NSi_2$	20	20.2
Hexamethyldisiloxane	162.4	$C_6H_{18}OSi_2$	7	16.58
Tetramethyldisiloxane	134.3	$C_4H_{14}OSi_2$	7	75.6
Tetramethylcyclotetrasiloxane	240.5	$C_4H_{16}O_4Si_4$	10	2.75
Tetraethoxysilane	208.3	$C_8H_{20}O_4Si$	17	1.15

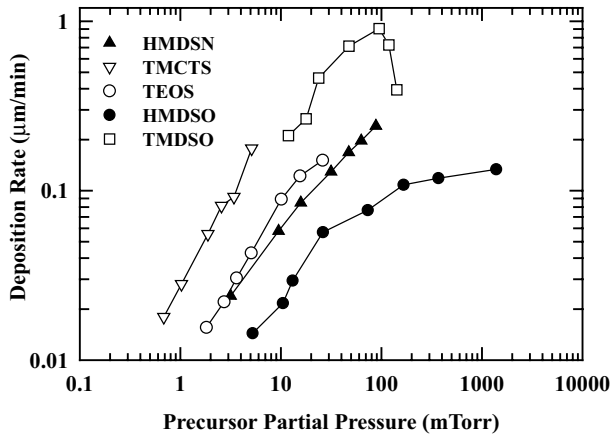

Figure 2. The dependence of the deposition rate on the precursor partial pressures.

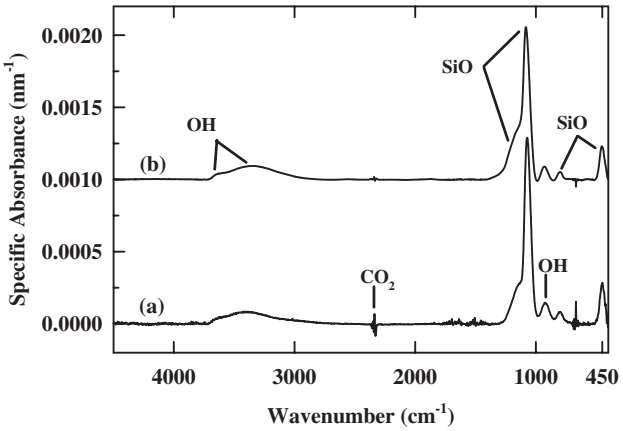

Figure 3. IR spectra of silicon dioxide films grown with HMDSN at (a) 0.023 μm min^{-1} and (b) 0.24 μm min^{-1}.

The results presented in figure 2 indicate that the deposition rate strongly depends on the specific precursor fed to the process. The growth rates observed with TMCTS, TEOS, HMDSN and HMDSO increase from about 0.015 to 0.2 μm min^{-1} with increasing precursor partial pressure. In the case of TMCTS, TEOS and HMDSN, the rates are approximately proportional to the amount of precursor fed. However, for HMDSO the rate gradually levels off at higher partial pressures. In contrast to these results, the growth rate obtained with TMDSO varies from 0.2 to 1.0 μm min^{-1} as the partial pressure increases from 10 to 100 mTorr. Above 100 mTorr, the deposition rate decreases with the TMDSO partial pressure.

Over the range of deposition rates shown in figure 2 there is no noticeable degradation in the material properties. With TMCTS and HMDSN, rates higher than 0.18 and 0.24 μm min^{-1} yield films with a white, chalky appearance. For TEOS, the films crack shortly after deposition at rates above 0.2 μm min^{-1}. Coatings deposited using TMDSO at a partial pressure above 140 mTorr exhibit a tacky texture and are easily removed with scotch tape.

The incorporation efficiency of the precursors into the glass films varies widely, as evidenced by the broad range of partial pressures examined for this process. This efficiency, which may be defined as the ratio of the moles of silicon in the film to the moles of precursor fed to the afterglow, is highest for TMCTS and TEOS, and lowest for HMDSO. In the case of TMCTS, this value increases from 7.2% to 9.6% as the growth rate rises from 0.02 to 0.18 μm min^{-1}. However, for TEOS, this trend reverses and the efficiency falls from 9.4% to 6.3% as the rate increases from 0.016 to 0.15 μm min^{-1}. With HMDSO, the incorporation efficiency ranges from 1.5% to 0.05% at growth rates between 0.014 and 0.13 μm min^{-1}. For HMDSN and TMDSO, the average incorporation efficiencies are 2.8% and 6.6%, respectively.

3.2. Film composition and structure

The refractive index measured for the SiO_2 films does not show a strong dependence on the precursor type and partial pressure. A value of 1.47 $\pm$ 0.03 is observed for TMCTS, TEOS, HMDSO and HMDSN. This refractive index is consistent with that reported for SiO_2 films deposited in low-pressure PECVD processes [13, 29, 30]. On the other hand, films produced from TMDSO at rates exceeding 0.7 μm min^{-1} exhibit a refractive index of 1.41 $\pm$ 0.02. Other studies of SiO_2 PECVD have recorded a similar drop in the refractive index, and have ascribed it to silicon–carbon bonds and voids in the films [31, 32].

Infrared absorbance spectra of films deposited with HMDSN at rates of 0.023 and 0.24 μm min^{-1} are presented in figure 3. The specific absorbance was obtained by dividing $-\log(I/I_0)$ by the film thickness. The peaks at 1075, 800 and 450 cm^{-1} are due to the asymmetric stretching, bending and rocking modes of siloxane bridges [13, 25, 33, 34]. The broad shoulder at $\sim$1150 cm^{-1} is also due to the stretching modes of the siloxane bridges [13, 34]. As is common with SiO_2 films grown at reduced temperature, the IR spectra also contain features attributed to hydroxyl groups. The peak at 930 cm^{-1} is due to O–H deformations, while the broad band and shoulder at 3400 and 3650 cm^{-1} are due to O–H stretching vibrations of hydrogen-bonded and isolated hydroxyl groups [13, 25]. Examination of the spectra in the figure reveals that no C–O, Si–H or C–H stretching modes at 1750, 2250 or 2900 cm^{-1} are detected at either deposition rate [13, 35–37].

Subtle differences are evident in the IR spectra of the glass films grown with HMDSN at the low and high deposition rates. The total area of the hydroxyl band between 2600 and 3600 cm^{-1} is 20% larger for the film deposited at 0.24 μm min^{-1}. Furthermore, the centre of this band is shifted 60 cm^{-1} to lower wavenumbers, presumably owing to increased contributions from hydrogen-bonded OH groups. The frequency of the Si–O–Si stretching vibration is 1070 cm^{-1} at 0.023 μm min^{-1} compared with 1082 cm^{-1} at 0.24 μm min^{-1}. Furthermore, the area of this peak is 26% smaller, while the high-frequency shoulder is 240% larger, for the higher growth rate compared with the lower one. These changes in the Si–O stretching modes are an indication of a slightly increased porosity in the SiO_2 film [13, 38].

Infrared spectra of films deposited with TCMTS, TEOS and HMDSO at their respective maximum deposition rates of approximately 0.15 μm min^{-1} are shown in figures 4(*a*) and (*b*) along with spectra for films grown with TMDSO at rates of 0.22 and 0.91 μm min^{-1}. The material deposited from TEOS and TMCTS exhibits O–H and Si–O–Si vibrations at 3650,

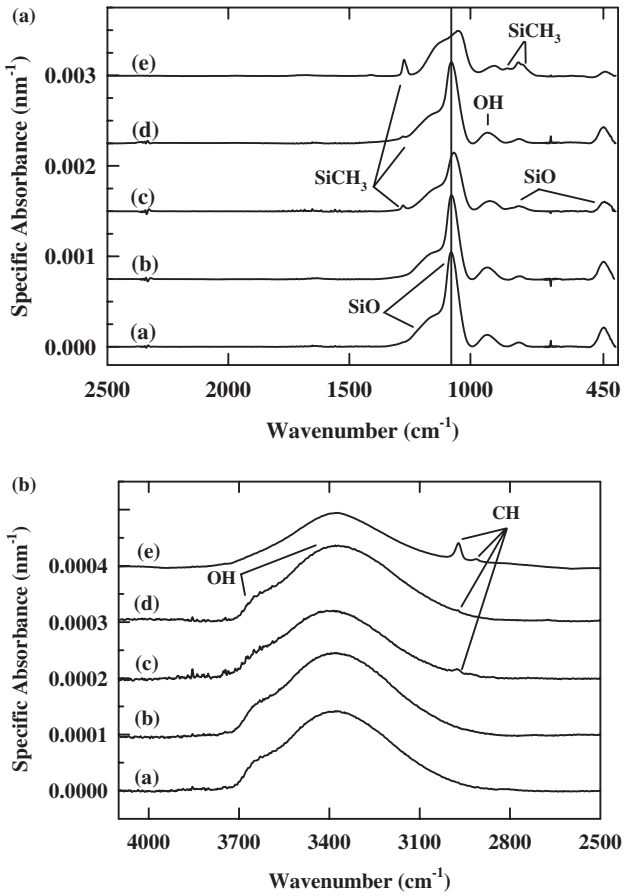

Figure 4. IR spectra of films deposited with (a) TCMTS at 0.18 μm min^{-1}, (b) TEOS at 0.15 μm min^{-1}, (c) HMDSO at 0.13 μm min^{-1}, (d) TMDSO at 0.21 μm min^{-1} and (e) TMDSO at 0.91 μm min^{-1}.

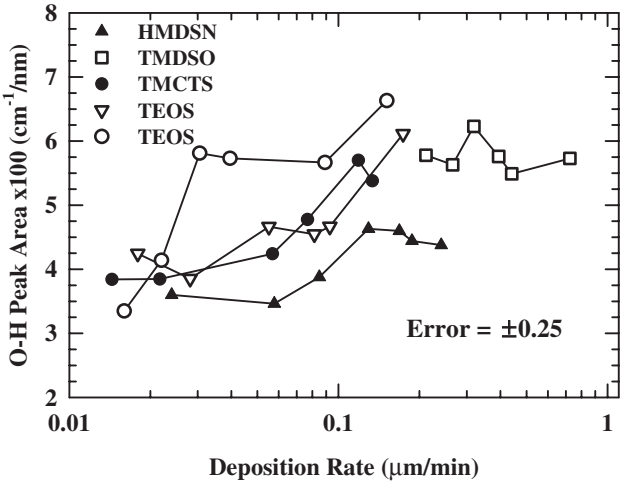

Figure 5. The dependence of the area of the OH vibrational band on the deposition rate for the different silicon precursors.

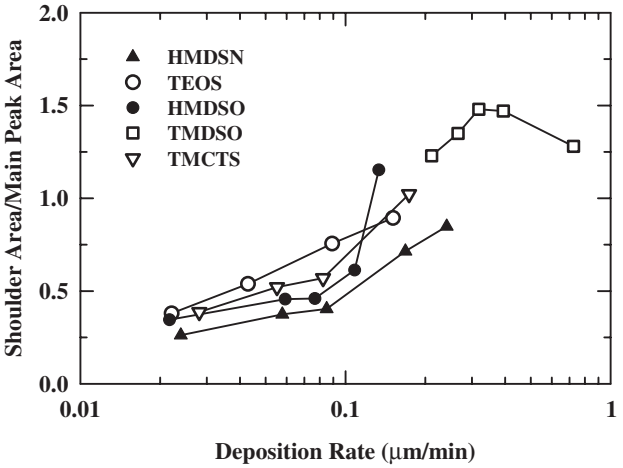

Figure 6. The trend in the 'film porosity' as a function of the deposition rate for the different silicon precursors.

3400, 1150, 1075, 800 and 450 cm^{-1}, which are characteristic of PECVD silicon dioxide. On the other hand, with TMDSO and HMDSO, a C–H bending mode is observed at 1275 cm^{-1}, which is due to the presence of methyl groups attached to silicon [37, 39–40]. Also, the C–H stretching modes at ~2900 cm^{-1} is observed in figure 4(*b*). These features are not present in films grown at rates at or below 0.10 μm min^{-1} with HMDSO. The IR spectra of films deposited at the maximum growth rate with TMDSO show a distribution of bands that are significantly different from those shown by the spectra of the other films. In particular, the siloxane peaks at 1075, 800 and 450 cm^{-1} are greatly reduced in intensity, while the shoulder at 1150 cm^{-1} is broader and more intense. Small peaks are discernible at 840 and 780 cm^{-1} as well. These changes are attributed to increased porosity and methyl–silicon bonding in the films [11, 37– 40].

Hydroxyl impurities are present in all the films deposited with the organosilane precursors. Since these groups weaken the glass-like structure of the coatings, they represent an important basis for comparison. It should be noted that the hydroxyl groups could either be incorporated into the films during growth or be the result of moisture uptake from the air after the samples were deposited. As will be shown below, the hydroxyl content correlates with the porosity of the films. Shown in figure 5 are the integrated peak areas of the hydroxyl stretching bands between 2700 and 3775 cm^{-1}. One sees a general trend of increasing hydroxyl content with deposition rate. For films deposited with TMDSO, the OH peak areas range from 0.055 to 0.063. For films deposited with TEOS, the OH peak area ranges from 0.03 at 0.016 μm min^{-1} to 0.07 at 0.15 μm min^{-1}. In contrast, films grown using HMDSN had slightly lower hydroxyl content, i.e. peak areas of 0.035 to 0.045 and showed a much weaker dependence on deposition rate. Using the method detailed by Chapple-Sokol *et al* [41], the hydrogen concentrations are estimated to range between 11.0 and 23.0 at% for TEOS and 13.0 and 16.0 at% for HMDSN. For a constant deposition rate of 0.15 μm min^{-1}, the OH peak area decreases with the precursor type in the following order: TEOS > TMCTS > TMDSO > HMDSO > HMDSN.

The ratio of the shoulder area of the Si–O stretching mode at ~1150 cm^{-1} to the primary peak area at ~1075 cm^{-1} has been correlated with the degree of porosity of silicon dioxide films [38]. The trends associated with this ratio are illustrated in figure 6. In the graph, the *y*-axis values were calculated by deconvoluting the Si–O stretching region into two peaks

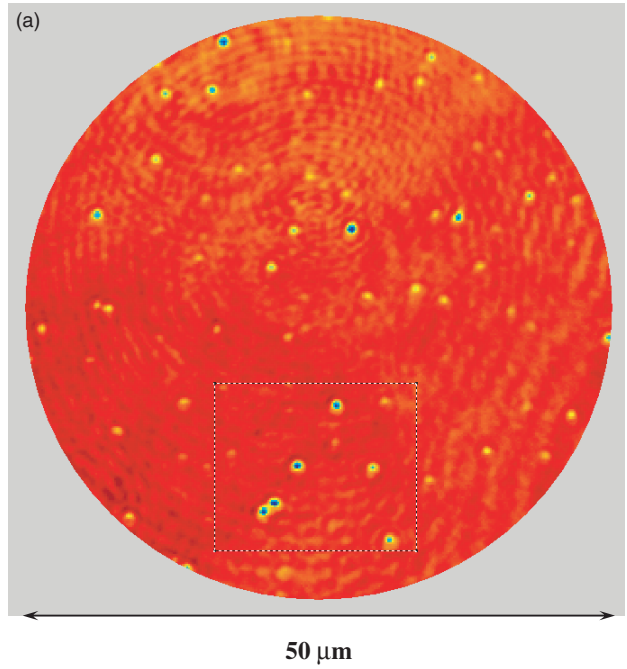

Figure 7. (*a*) Three-dimensional surface image of a 650 nm-thick film grown at a rate of 0.21 μm min^{-1} using TMDSO; (*b*) shows the magnified image of the surface.

(This figure is in colour only in the electronic version)

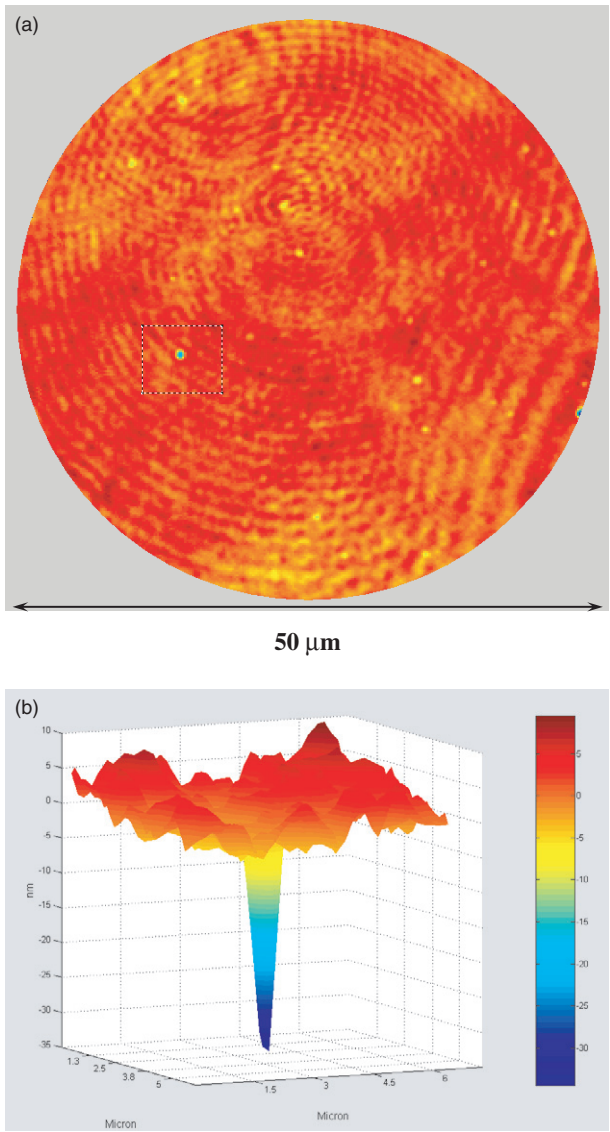

Figure 8. (*a*) Three-dimensional surface image of a 650 nm-thick film grown at a rate of 0.24 μm min^{-1} using HMDSN; (*b*) shows the magnified image of the surface.

(This figure is in colour only in the electronic version)

located at 1075 ± 5 and 1150 ± 10 cm^{-1}. Inspection of the graph reveals that there is an increase in porosity with growth rate, and that films deposited using TMDSO have higher degrees of porosity than those obtained with the other precursors. Of these, HMDSN produces the least porous material when compared with TEOS, HMDSO and TMCTS at equal deposition rates.

Further evidence of the differences in the porosity of the films can be seen in images recorded with the optical profiler. A three-dimensional surface image of a film, grown 650 nm thick at 0.21 μm min^{-1} with TMDSO, is presented in figure 7. The image shows a number of pits that are approximately 1.0 μm in diameter and 40–130 nm deep. The number density of these pits is approximately 0.038 μm^{-2}. This is in contrast to the surface profile of a film of equal thickness, but deposited with HMDSN at a rate of 0.24 μm min^{-1}. The image of this coating is shown in figure 8. It is significantly less porous. The number density of pits is 0.014 μm^{-2} and their maximum depth is only 35 nm.

3.3. Mechanical performance

The scratch tests performed on silicon wafers indicate that the mechanical properties of the films deposited with HMDSN do not depend strongly on growth rate. Shallow scratch depths are measured over the entire range of rates from 0.023 to 0.24 μm min^{-1}. For HMDSO, TMCTS and TEOS, films deposited at rates below 0.1 μm min^{-1} display good scratch resistance, with the screwdriver tip penetrating less than 13 nm into the films. Beyond 0.1 μm min^{-1}, the hardness drops and deep scratch penetration is observed. For TMDSO, deep scratches are recorded over the whole range of deposition rates, between 0.21 and 0.91 μm min^{-1}.

Table 2. Pencil hardness results of glass films on plastic.

Precursor	Deposition rate (μm min^{-1})	Film thickness (μm)	Pencil hardness
HMDSN	0.075	0.5	4H
HMDSN	0.075	1.0	4H
HMDSN	0.24	0.5	HB
HMDSN	0.24	1.5	4H
TMDSO	0.21	0.5	HB
TMDSO	0.21	1.5	3H
TMDSO	0.91	0.5	HB
TMDSO	0.91	1.5	HB

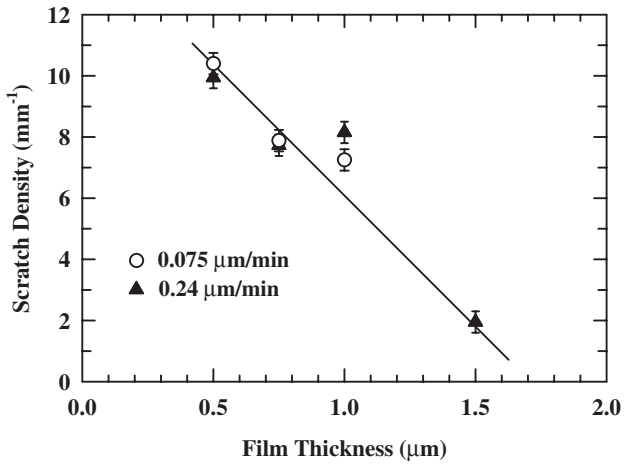

Figure 9. Linear scratch density recorded after steel-wool abrasion of glass films grown with HMDSN.

Further hardness testing was conducted on plastic substrates using HMDSN and TMDSO. Two deposition rates were investigated for each precursor: 0.075 and 0.24 μm min^{-1} for HMDSN, and 0.21 and 0.91 μm min^{-1} for TMDSO. In addition, coatings varying in thickness from 0.5 to 1.5 μm were examined. The results of the pencil hardness tests are presented in table 2. With HMDSN at 0.075 μm min^{-1}, the hardness does not show a dependence on thickness, as both films have a rating of 4H. However, there is a dependence on film thickness at 0.24 μm min^{-1}. In this case, the hardness rating of the 0.5 μm-thick film is HB, while that of the 1.5 μm-thick film is 4H. With TMDSO, the hardness at 0.21 μm min^{-1} also increases with film thickness. However, the material is softer and the 1.5 μm-thick film achieves only a 3H rating. At the maximum TMDSO deposition rate, the films exhibit a constant pencil hardness of HB, independent of the thickness.

Shown in figures 9 and 10 are the linear scratch densities caused by steel wool abrasion of films grown with HMDSN and TMDSO, respectively. In the former case, the number of scratches decreases as the film thickness increases, independent of growth rate. The 1.5 μm-thick film exhibits only 2 scratches per millimetre. On the other hand, films deposited with TMDSO show an effect of growth rate on abrasion resistance. At 0.91 μm min^{-1}, the scratch density equals 11 mm^{-1} for all films between 0.5 and 1.5 μm thick. In contrast, at 0.21 μm min^{-1}, the number of scratches declines

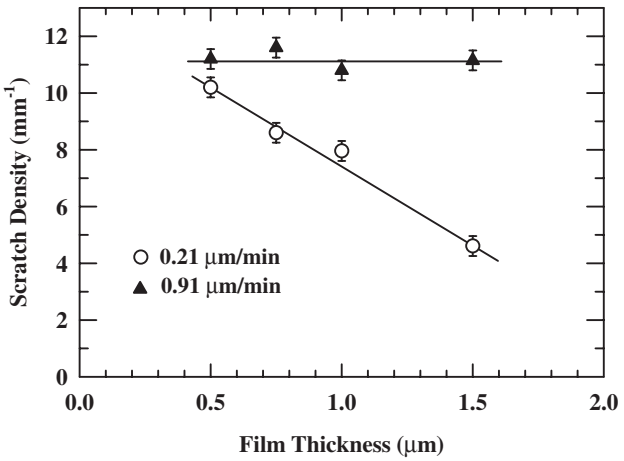

Figure 10. Linear scratch density recorded after steel-wool abrasion of glass films grown with TMDSO.

with thickness to about 4 mm^{-1} at 1.5 μm. Comparison of these data with the results presented in figures 4–6 suggests that the poor abrasion resistance of the glass deposited at 0.91 μm min^{-1} is most likely to be due to the incorporation of methyl groups into the film.

4. Discussion

The results described above demonstrate that a chamberless, remote plasma deposition process may be used to generate abrasion-resistant glass coatings on plastic. The properties of these coatings depend on the type and the amount of organosilane precursor fed to the process. The range of deposition rates achieved with different precursors spans two orders of magnitude. High quality films without visible defects, such as cracking or chalkiness, can be obtained with TEOS, TMCTS and HMDSO at rates ranging from 0.02 to 0.15 $\pm$ 0.02 μm min^{-1}, and with HMDSN at rates of up to 0.24 μm min^{-1}. Glass may be deposited with TMDSO at a significantly higher rate of 0.91 μm min^{-1}. However, the material exhibits poor abrasion resistance.

It is difficult to compare the deposition rates observed in this study with those reported in the literature due to wide variations in plasma source design and operation. In the recent literature, the following maximum rates have been reported: 1.0 μm min^{-1} using HMDSO and TMCTS [42], 10.0 μm min^{-1} with TEOS [43], 0.4 μm min^{-1} with HMDSN [40] and 1.3 μm min^{-1} with TMDSO [31]. Most of these studies utilized electron cyclotron resonance (ECR) plasmas operating at pressures below 100 mTorr and in the presence of high energy electrons at densities between 10^{11} and 10^{13} cm^{-3} [7, 40, 42]. Since the precursor molecules are fed directly into the discharge they are subject to dissociation by both neutral chemistry and electron impact [7]. In the studies utilizing TEOS and TMDSO, the precursors were fed directly into a low-pressure capacitive discharge and were exposed to the same dissociation pathways as in the ECR plasma [31]. However, only neutral chemistry occurs in the atmospheric plasma deposition process. This would explain

why the low-pressure plasma processes generally yield higher deposition rates than those observed here.

The results obtained in this study clearly show that the impurity concentration in the glass films depends on the organosilane precursor used and the deposition rate. The IR spectra presented in figures 3 and 4 reveal significant quantities of unreacted methyl groups in material grown with TMDSO and HMDSO. For the former precursor, the number of CH_3 species rises dramatically when the growth rate is increased from 0.21 to 0.91 μm min^{-1}. The hydroxyl content of the films in general increases with the deposition rate, as illustrated in figure 5. Nevertheless, at a rate of near by 0.2 μm min^{-1}, the glass film produced with HMDSN contains significantly less OH than the films grown using the other precursors. The trends in film porosity, as indicated by the ratio of the IR band at 1150 cm^{-1} to that at 1075 cm^{-1} (figure 6), mirror that of the hydroxyl content. Porosity increases with deposition rate, while at a fixed rate near 0.2 μm min^{-1}, the films made with HMDSN are less porous than those made with other precursors. This can be seen also in the optical images of the films grown with TMDSO and HMDSN in figures7 and 8, respectively.

The impurity concentration in the glass coatings has a strong impact on their mechanical properties. Films generated with TMDSO at a rate of 0.91 μm min^{-1}, and containing significant quantities of unreacted methyl groups, exhibit an HB value in pencil hardness as well as high scratch densities after steel wool abrasion. The effect of hydroxyl impurities may be illustrated by comparing 1.5 μm-thick films grown at ∼0.2 μm min^{-1} using HMDSN and TMDSO. The former precursor generates less OH in the film, resulting in 4H hardness and a scratch density of 2 mm^{-1}. In contrast, the film grown with TMDSO exhibits a 3H pencil hardness and a scratch density of 4.5 mm^{-1}. Previous work on plasma-assisted deposition of glass films using organosilane precursors has observed a strong effect of impurities on abrasion resistance [10, 11, 42]. In these studies, it was concluded that impurities disrupt the Si–O–Si bonding network, leading to more porous films that are softer and more easily scratched.

As one would expect, the mechanical properties of the glass films improve with the thickness of the layers. For example, comparing films grown with HMDSN at 0.24 μm min^{-1}, the pencil hardness is HB and the scratch density is 10 mm^{-1} for the 0.5 μm-thick coating, whereas they are 4H and 2 mm^{-1}for the 1.5 μm-thick coating. These same trends have been observed previously [6, 10]. Evidently, a minimum coating thickness is needed for the material to assume the mechanical properties of the glass and not the underlying plastic substrate.

5. Conclusions

An atmospheric plasma source has been used to deposit glass-like coatings on plastic without the use of a chamber. The organosilane precursor utilized in the process has a large impact on the film growth rate, composition and physical structure. We have found that coatings closely resembling SiO_2, with minimal OH and CH_x impurities, provide superior hardness and abrasion resistance. The silazane precursor, HMDSN, shows promise for producing this material at a reasonable deposition rate.

Acknowledgment

Funding for this research was provided by a grant from Motorola, Inc.

References

[1] Heller A 1999 *Sci. Technol. Rev.* **9** 20
[2] Chwang A B *et al* 2003 *Appl. Phys. Lett.* **83** 413
[3] Vaeth K M and DiCillo J 2003 *J. Polym. Sci.* B **41** 2715
[4] Hong Y T, He Z Q, Lennhoff N S, Banach D A and Kanicki J 2004 *J. Electron. Mater.* **33** 312
[5] Cheng I C and Wagner S 2003 *IEE Proc.* **150** 339
[6] Katsamberis D, Browall K, Iacovangelo C, Neumann M and Morgner H 1998 *Prog. Org. Coat.* **34** 130
[7] Lieberman M A and Lichtenberg A J 1994 *Principles of Plasma Discharges and Materials Processing* (New York: Wiley Interscience)
[8] Schaepkens M, Selezneva S, Moeleker P and Iacovangelo C D 2003 *J. Vac. Sci. Technol.* A **21** 1266
[9] Ward L J, Schofield W C E, Badyal J P S, Goodwin A J and Merlin P J 2003 *Langmuir* **19** 2110
[10] Li H, Sharma R K, Zhang Y, Tay A A O, Kang E T and Neoh K G 2003 *Langmuir* **19** 6845
[11] Teshima K, Inoue Y, Sugimura H and Takai O 2002 *Thin Solid Films* **420–421** 324
[12] Jeong J Y, Park J Y, Henins I, Babayan S E, Tu V J, Selwyn G S, Ding G and Hicks R F 2000 *J. Phys. Chem.* **104** 8027
[13] Babayan S E, Jeong J Y, Schütze A, Tu V J, Moravej M, Selwyn G S and Hicks R F 2001 *Plasma. Sources. Sci. Technol.* **10** 573
[14] Babayan S E, Ding G and Hicks R F 2001 *Plasma Chem. Plasma Process.* **21** 505
[15] Babayan S E, Ding G, Nowling G R, Yang X and Hicks R F 2002 *Plasma Chem. Plasma Process.* **22** 255
[16] Nowling G R, Yang X, Moravej M, Agarwal R and Hicks R F 2004 *Plasma Sources Sci. Technol.* **13** 156
[17] Moravej M, Babayan S E, Nowling G R, Yang X and Hicks R F 2004 *Plasma Sources Sci. Technol.* **13** 8
[18] Nowling G R, Babayan S E, Jankovic V and Hicks R F 2002 *Plasma Sources Sci. Technol.* **11** 97
[19] Schumacher 2002 Tetramethylcyclotetrasiloxane MSDS
[20] Schumacher 2002 Tetraethoxysilane MSDS
[21] Mallinckrodt Inc. 2001 Hexamethyldisilazane MSDS
[22] Sigma-Aldrich 2002 Hexamethyldisiloxane MSDS
[23] Sigma-Aldrich 2002 Tetramethyldisiloxane MSDS
[24] Levine I N 1995 *Physical Chemistry* (New York: McGraw-Hill)
[25] Theil J A, Tsu D V, Watkins M W, Kim S S and Lucovsky G 1990 *J. Vac. Sci. Technol.* A **8** 1374
[26] GE Plastics 2002 LEXAN EXL1414 Datasheet
[27] ASTM D3363-00
[28] Yuan H Y, Lu X Y, Zeng Z H, Yang J W and Chen Y L 2004 *J. Appl. Polym. Sci.* **92** 2765
[29] Wolf S and Tauber R N 1986 *Silicon Processing for the VLSI Era, Vol. 1: Process Technology* (California: Lattice)
[30] Choi J K, Kim D H, Lee J and Yoo J B 2000 *Surf. Coat. Technol.* **131** 136
[31] Wu Q and Gleason K K 2003 *Plasma Polym.* **8** 31
[32] Barrell Y, Creatore M, Schaepkens M, Iacovangelo C D, Miebach T and van de Sanden M C M 2004 *Surf. Coat. Technol.* **180–181** 367

[33] Lucovsky G, Richard P D, Tsu D V, Lin S Y and Markunas R J 1986 *J. Sci. Technol.* A **4** 681
[34] Pai P G, Chao S S, Takagi Y and Lucovsky G 1986 *J. Vac. Sci. Technol.* A **4** 689
[35] Sawada Y, Ogawa S and Kogoma M 1995 *J. Phys. D: Appl. Phys.* **28** 1661
[36] Hanyaloglu B F and Aydil E S 1998 *J. Vac. Sci. Technol.* A **16** 2794
[37] Matsutani T, Asanuma T, Liu C, Kiuchi M and Takeuchi T 2000 *Surf. Coat. Technol.* **177–178** 365
[38] Chou J S and Lee S C 1995 *J. Appl. Phys.* **77** 1805
[39] Zywitzki O, Sahm H, Krug M, Morgner H and Neumann M 2000 *Surf. Coat. Technol.* **133–134** 555
[40] Sahli S, Rebiai S, Raynaud P, Segui Y, Zenasni A and Mouissat S 2002 *Plasmas Polym.* **7** 327
[41] Chapple-Sokol J D, Pliskin W A and Conti R A 1991 *J. Electrochem. Soc.* **138** 3723
[42] Qi Y, Xiao Z G and Mantei T D 2003 *J. Vac. Sci. Technol.* A **21** 1064
[43] Patrick W J, Schwartz G C, Chapple-Sokol J D, Carruthers R and Olsen K 1992 *J. Electrochem. Soc.* **139** 2604